Chaotic Modeling and Simulation (CMSIM) 1: 89-106 , 2013

Rotations-Expansion-Reflections Chaotic Modelling with Singularities in Higher Dimensions

Bernd Binder

Quanics, Salem, Germany
E-mail: binder@quanics.com,

Abstract: Rotation – Expansion – Translation – Reflection chaotic models show despite of its simple generators complex structures that resemble in 2 dimensions - without referring to any material property - well known fluid/flux vortex flow patterns as recently shown by Skiadas. Here the model is generalized and extended to $n > 2$ dimensions with $N = n(n-1)/2$ rotational degrees of freedom and the maximum of $L = n(n-1)(n-2)/2$ singularity rotations on the sphere and hyper sphere with rotation matrix operations given by the orthogonal group O(n), special orthogonal group SO(n), or Lie spin group Spin(n) with hierarchical relations. The radial distance to the singularities located on the rotation axes leads to the Skiadas power law rotation parameterized by a power exponent and rotation strength. Patterns often show characteristic flux lines emitted from a chaotic core near to a singularity. The non-commutative permutations of the non-abelian rotation group elements are relevant for encryption purposes.

Keywords: Chaotic modeling, Discrete map, Rotation-Translation, Rotation-Rotation, molecular interaction, v. Kármán Street, Dipole-dipole, Chaotic simulation, Chaotic encryption, Spin group.

1. Introduction

In quantum physics the spatial probability density and its symmetries are a basic concept to describe the evolution of observables obtained from stochastic (jump) processes in phase space. The Rotation – Expansion – Translation – Reflection pattern generation approach of Skiadas provides also for spatial density structures but from iterative difference equations generating more or less chaotic jumps [1, 2, 3]. The first results of Skiadas are very similar to v. Kármán Streets, see fig. 1, or even elliptic galaxies formations. Since a translation is a special case of a rotation with the rotation centre located at very large distances, applying subsequent rotations repeatedly around different rotation centres should also provide for interesting patterns, especially if the rotations are a function of a spatial distance with respect to one or more singularities, where rotations grow infinite due to a power law with negative exponent. We will focus in this paper onto the rotation-rotation chaotic phase jump processes on hyper-spherical loops with larger or smaller chaotic core regions, which depend on characteristic numbers and symmetries. Since the signal $\mathbf{p}_t$ jumps in hyper

Received: 14 July 2012 / Accepted: 30 October 2012

ISSN 2241-0503

space or on hyper spheres, the resulting patterns could be relevant to physics and quantum spin groups in higher dimensions [4]. First we will introduce the rotation-translation approach in two dimensions (2-D) with one or more singularities and then replace the translation by another rotation and generalize to *n* dimensions on (hyper) spherical surfaces. After generating some new chaotic jump pattern by extending the Skiadas algorithm and relating it to proper physics attributes, some new input came from discussions during and shortly after the conference, especially from some authors of references [1]-[6].

2. The 3-D Expansion/Rotations/Translation Model

In 3-D Euclidian space we can map the Skiadas model onto the sphere with 2 or 3 rotations. A vector coordinate $\mathbf{p}_t$ will describe the signal location at a time *t* and after one jump time interval τ at $\mathbf{p}_{t+\tau}$, where the signal starts at $\mathbf{p}_0$. First we apply a expansion/reflection matrix $\mathbf{E}$, then apply $N = 3$ different rotation in planes $\mathbf{P}_i$, $i = 0,1,..,N-1$, each containing $l = 0,1,..,m_i - 1$ singularities $\mathbf{s}_{i,l}$ defining the rotation centre. At this location the axes $\mathbf{X}_{i,l}$ intersect $\mathbf{P}_i$ orthogonally. The rotation angles $\vartheta_{i,l}$ are given by the Skiadas power-law [1]

$$\vartheta_{i,l} = 2\pi c_i \left(\frac{|\mathbf{v}|\tau}{|\mathbf{p}_t - \mathbf{s}_{i,l}|} \right)^2, \tag{1}$$

with distance between signal and singularity coordinates $|\mathbf{p}_t - \mathbf{s}_{i,l}|$, power exponent value usually in the range 1-3, and coupling constants c_i. We have chosen a form producing patterns linearly scaling with the jump distance $|\mathbf{v}|\tau$ while preserving shape. For one singularity per dimension $m_i = 1$ the three rotations with angles ϑ_i are computed by the rotation matrices $\mathbf{R}_i$ applied in a given permutation sequence. We take a proper coordinate system diagonalizing $\mathbf{E}$ with pure diagonal expansion/reflection components $e_{ij} = 0$ for $i \neq j$ and $|e_{xx}| = |e_{yy}| = |e_{zz}| > 0$. For this case we will use the short notation $\mathbf{E} = \mathrm{ED}(e_{xx}, e_{yy}, e_{zz})$, a negative sign shows a so-called reflection in the corresponding coordinate. These components and boundary conditions provide for the basic 3-D recurrent algorithm and difference equation as a simple extension to [1, 2, 3] generating one jump with distance $|\mathbf{v}\tau|$ after the interval τ. If we assume orthogonal rotation axes with rotation matrices $\mathbf{R}_i$ elements of the SO(3) rotation group, we have a common rotation centre located at $\mathbf{r}$ as the intersection of the rotation axes with one singularity from every dimension ($m_i = 1$) and orthogonal axes $\mathbf{X}_{0,0} \perp \mathbf{X}_{1,0} \perp \mathbf{X}_{2,0}$, where the chaotic map given by

$$\mathbf{p}_{t+\tau} = \mathbf{v}\tau + \mathbf{R}_2\left[\mathbf{R}_1\left[\mathbf{R}_0\left[\mathbf{E}\left[\mathbf{p}_t - \mathbf{r}\right]\right]\right]\right] + \mathbf{r}. \tag{2}$$

To get pure rotations, the straight translation shift $|\mathbf{v}\tau|$ in eqs. (2) and (1) could be approximated by constant orbital rotations in one dimension with label j and $|\mathbf{r}_j|\vartheta_j = 2\pi|\mathbf{v}\tau|$ leading to the Skiadas rotations coupling

$$\vartheta_{i,l} = 2\pi c_i \left(\frac{|\mathbf{r}_j|\vartheta_j}{2\pi|\mathbf{p}_t - \mathbf{s}_{i,l}|} \right)^{d_{i,l}}, \text{ in 3-D we usually take } d_j = 2, \quad (3)$$

where the coupling factor c_i can be varied in a wide range. Spin is given by an orbital rotation with label $i = j$ that has one singularity at the centre $\mathbf{s}_{j,0} = (0,0,0)$, where

$$\left(\frac{\vartheta_j}{2\pi} \right)^{1-d_j} = c_j \frac{|\mathbf{r}_j|^{d_j}}{|\mathbf{p}_t|^{d_j}}, \text{ for } d_j = 1 \text{ simply } |\mathbf{p}_t| = c_j |\mathbf{r}_j|. \quad (4)$$

The iterative 3-D difference equation (2) for one start point or delta distribution $\mathbf{p}_0 = \mathbf{p}_{t=0}$ with 3 singularities and 3 orthogonal rotations is now

$$\mathbf{p}_{t+\tau} = \mathbf{R}_{\vartheta_2}\left[\mathbf{R}_{\vartheta_1}\left[\mathbf{R}_{\vartheta_0}\left[\mathbf{E}[\mathbf{p}_t - \mathbf{r}]\right]\right]\right] + \mathbf{r}. \quad (5)$$

To obtain interesting patterns on the spherical surface we set $\mathbf{R}_{3,1} = \mathbf{R}_\theta$ as the constant longitude or orbital advance, and $\mathbf{R}_{1,2} = \mathbf{R}_\vartheta$ for the altitude. Both rotations rotate around singularities given by

- $m_{3,1} = 1$, one longitude rotation $\mathbf{R}_{3,1} = \mathbf{R}_\theta$ rotating around $\mathbf{s}_{3,1,1} = (0,0,0)$ with power law exponent $d_{3,1,1} = 0$ and rotation/coupling strength $c_{3,1,1} = 2\pi jM^{-1}$,
- $m_{1,2} = 1$, one latitude rotation $\mathbf{R}_{1,2} = \mathbf{R}_\vartheta$ rotating around $\mathbf{s}_{1,2,1} = (0,0,1)$ with power law exponent $d_{1,2,1} = 2$ and rotation/coupling strength $c_{1,2,1} = 2\pi k^{-2}M^{-2}$.

As an example, a two-angle rotation and signal position $\mathbf{p}_t$ subject to rotation in 3-D spherical coordinates φ, ϕ and singularity rotations $\vartheta_0 = \vartheta$, $\vartheta_1 = \theta$, is given by

$$\mathbf{p}_t(\varphi,\phi) = \begin{pmatrix} \sin\varphi\cos\phi \\ \cos\phi \\ \sin\varphi\sin\phi \end{pmatrix}, \mathbf{R}(\theta,\vartheta) = \begin{pmatrix} \cos\vartheta\cos\theta & -\sin\vartheta\cos\theta & \sin\theta \\ \sin\vartheta & \cos\vartheta & 0 \\ -\cos\vartheta\sin\theta & \sin\vartheta\sin\theta & \cos\theta \end{pmatrix}.$$

With one singularity located at $\mathbf{s}_0 = (0,0,1)$ with $d = 2$ and one at the centre $\mathbf{s}_1 = (0,0,0)$ with $d = 0$ we get the two scalar rotations in spherical coordinates

$$\vartheta = c\frac{\theta^2}{4\pi(1-\sin\varphi\sin\theta)},\ \theta = \frac{2\pi j}{M},\ c = \frac{1}{j^2k^2}. \tag{6}$$

3. Hyper-Sphere Expansion-Reflection-Rotations Map

The extension to the n-*D* signal map $\mathbf{p}_t \to \mathbf{p}_{t+\tau}$ with rotations embedded in *n*-D Euclidean space for $n \geq 3$ is straight forward. The matrix operations are based on the orthogonal group O(*n*), or the Lie spin group Spin(*n*) as the double cover of the special orthogonal group SO(*n*) defining the $n \times n$ rotation matrices $\mathbf{R}_{a,b}$. The number of rotational degrees of freedom and number of orthogonal rotation planes $\mathbf{P}_{a,b}$ is

$$N(n) = \binom{n}{2} = \frac{n(n-1)}{2},\ N(n \geq 2) = 1, 3, 6, 10, 15, 21, 28, 36, 45, \ldots. \tag{7}$$

One plane can have orthogonal axes $\mathbf{X}_l$ intersecting the plane at the singularity locations $\mathbf{s}_{a,b,l}$, l labels all orthogonal axes with $l \neq a, l \neq b$. We rotate on this plane if the rotation plane has at least one orthogonal intersection $m_{a,b} > 0$ at the singularity locations. The maximum number of singularities per dimension is $m_{a,b} = (n-2)$, if $m_{a,b} = 0$ there are no singularities and no rotations in $\mathbf{P}_{a,b}$. So the total number of possible orthogonal axis intersections for all planes and the maximum number of singularities is $L = (n-2)N = n(n-1)(n-2)/2$. There is a set of *N* orthogonal matrices $\mathbf{R}_{a,b}{}^T = \mathbf{R}_{b,a} = \mathbf{R}_{a,b}{}^{-1}$ with $\det \mathbf{R}_{a,b} = 1$ defining the special orthogonal group SO(*n*) given according to [4] by

$$\mathbf{R}_{a,b}(\vartheta_{a,b,l}) = \begin{bmatrix} r_{i,j} \begin{vmatrix} r_{a,a} = \cos(\vartheta_{a,b,l}) \\ r_{b,b} = \cos(\vartheta_{a,b,l}) \\ r_{a,b} = -\sin(\vartheta_{a,b,l}) \\ r_{b,a} = \sin(\vartheta_{a,b,l}) \\ r_{j,j} = 1,\ j \neq a,\ j \neq b \\ r_{i,j} = 0,\ \text{elsewhere} \end{vmatrix} \end{bmatrix}, \tag{8}$$

with trace $n - 2\left[1 - \cos(\vartheta_{a,b,l})\right]$ and angles $\vartheta_{a,b,l}$, $l \neq a, l \neq b$. The signal is located on the hyper-spheres. The sequence of orthogonal matrices rotating a vector $\mathbf{x}_t$ in Euclidean space must be ordered

$$\mathbf{R}_{A,B}\left[\mathbf{x}_t\right] = \mathbf{R}_{\ldots}\left[\ldots\left[\mathbf{R}_{a,b}\left[\ldots\left[\mathbf{R}_{\ldots}\left[\mathbf{x}_t\right]\right]\right]\right]\right], \tag{9}$$

covering all possible rotations or a subset as a permutation. Building the chaotic map with an *n*-D expansion/reflection $\mathbf{E}$ then applying the rotation sequence $\mathbf{R}_{A,B}$ we have

$$\mathbf{p}_{t+\tau} = \mathbf{R}_{A,B}\left[\mathbf{E}\left[\mathbf{p}_t - \mathbf{r}\right]\right] + \mathbf{r} \,. \tag{10}$$

We are left to specify the generalized rotation angles $\vartheta_{a,b,l}$, the matrix coefficients for a rotation $\mathbf{R}_{a,b}(\vartheta_{a,b,l})$, the number of singularities per dimension $m_{a,b}$, and the temporal order of rotations. The angles $\vartheta_{a,b,l}$ corresponding to $\mathbf{s}_{a,b,l}$ will have with strength $c_{a,b,l} \in \mathbb{R}$, metric distance $\left|\mathbf{p}_t - \mathbf{s}_{a,b,l}\right|$, and power exponent $d_{a,b,l} \geq 0$ a form given by

$$\vartheta_{a,b,l} = 2\pi c_{a,b,l}\left(\frac{\left|\mathbf{v}\,\tau\right|}{\left|\mathbf{p}_t - \mathbf{s}_{a,b,l}\right|}\right)^{d_{a,b,l}} \,. \tag{11}$$

To systematically generate meaningful setup values in higher dimensions providing for interesting patterns for $n > 2$ with physical relevance, we recommend for simplicity to take a Gauss-type classical coupling field gradient power exponent

$$d_{a,b,l} = n - 1 \,, \tag{12}$$

where the gradient power exponent is the Gauss' law field strength exponent plus 1 (for 3-D we have $d_{a,b,l} = 2$, see below). But of course, as Skiadas has shown there are several exponents that can lead to nice patterns. The power law coupling strength is scaling with the field gradient power exponent and coupling number *k*

$$c_{a,b,l} = k^{-d_{a,b,l}} \,. \tag{13}$$

The temporal order of rotations $\mathbf{R}_{a,b}$ part of the global sequence $\mathbf{R}_{A,B}$ as a permutation sequence must be given in order to setup the map and reproduce results. For the purposes of this paper we let run a in an outer loop from 0 to $n-1$, then b in the next inner loop from $a+1$ to $n-1$ covering the $N = n(n-1)/2$ orthogonal rotation planes $\mathbf{P}_{a,b}$ with orthogonal matrices $\mathbf{R}_{a,b}$, and finally l in the most inner loop from 0 to $n-1$ with $l \neq a, l \neq b$, since every plane has $n-2$ orthogonal axes intersecting at the singularities providing for the total number of singularities rotations $L = n(n-1)(n-2)/2$.

4. Results

4.a Four basic 2-D rotation-translation types with radial power -3

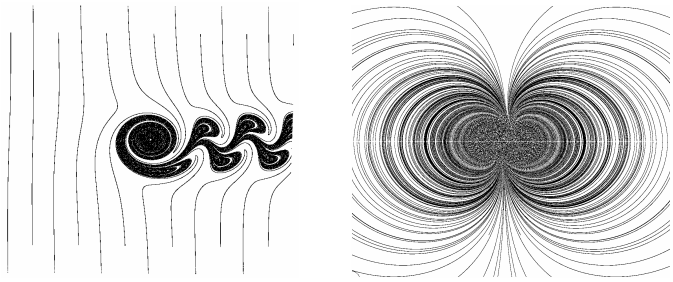

Fig. 1. Left (Skiadas [1]): EC = (1,-1). Right EC = (-1,1) , randomized starts.

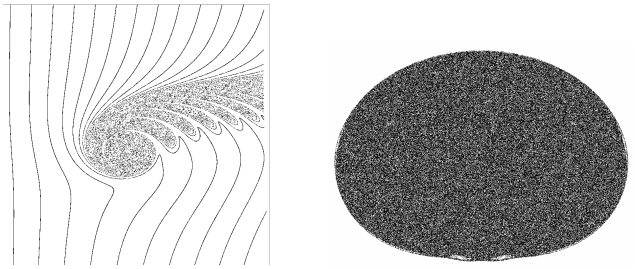

Fig. 2. Left (Skiadas [3]): EC = (1, 1). Right EC = (-1,-1), randomized starts.

4.b Periodic boundary (at $d_0 = 16\tau$) in 2-D at power -3

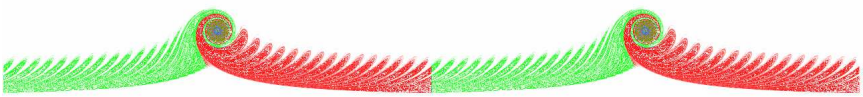

Fig. 3. EC = (1, 1), if distance $x > d_0$ then $x \rightarrow x$ - 2-D_0, $y \rightarrow y$, slightly random.

Fig. 4. The periodic Skiadas pattern, same parameter like fig.3 but EC = (1, -1).

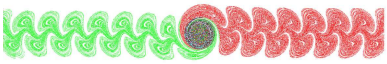

Fig. 5. Parity change for EC = (1, -1): if distance $x > d_0$, then $x \rightarrow -x$ $y \rightarrow y$.

4.c Helical twist and 2-D rotation in 3-D

Fig. 6. 3-D cyclic within $d_0 = 16\tau$, power -3, with extra double-helix rotation $\psi = 5\pi x / d_0$ proportional to distance x, EC = (1, -1), randomized starts.

4.d. Multi-singularity and multi-expansion in 2-D, overlapping patterns

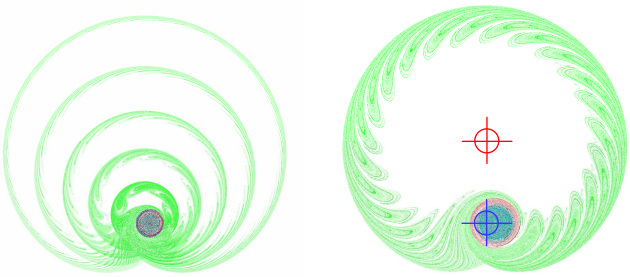

Fig. 7. Two equal singularities: positive at (0,0) and negative located at (0, 2j), j = 1,2,3,4,5, power -3, EC = (1, 1). Right: enlarged j = 1 with one positive (blue) and one negative (red) singularity.

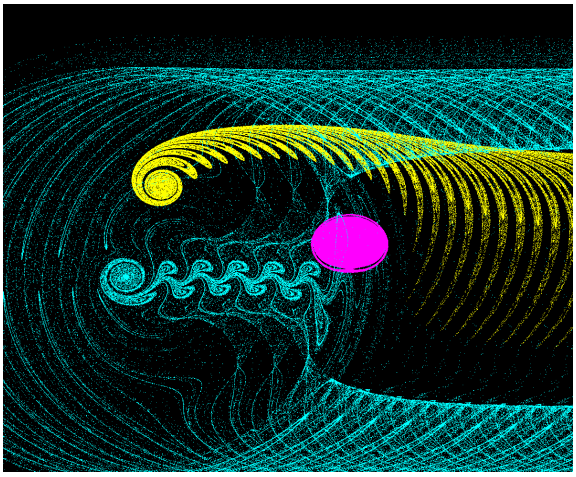

Fig. 8. Three singularities at different locations, power -3, multi expansion, 3 different EC: (1, 1) and (1, -1) and (-1, -1), randomized starts.

4.e Rotation-Rotation in 3-D, rotation centre at (0,0,0), singularity at (0,0,1)

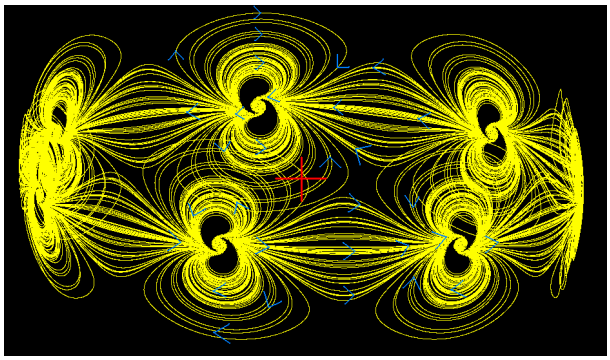

Fig. 9. Dipole ring, power -2, $M = 7$, EC = (1,-1, 1), $k = 8$, slightly random. Flow directions are indicated by blue arrows.

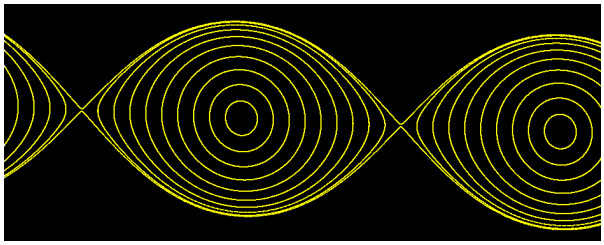

Fig. 10. Rings deformed to a wave, power -2, $M = 113$, EC = (1, 1, 1), $k = 20$, $\vec{s}_{0,i} = (x_i, \sqrt{1-x_i^2}, 1)$, $x_i = i / M / 10, i = 1,2,...,10$, $j = 1$.

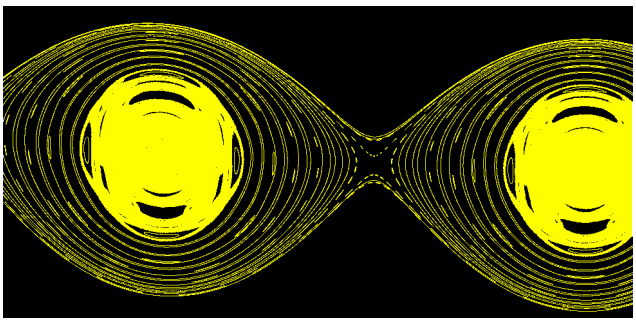

Fig. 11. Similar to fig. 10 but chaotic core with $k = 2$, power -2, $M = 13$, EC = (1, 1, 1), $\vec{s}_{0,i} = (x_i, \sqrt{1-x_i^2}, 1)$, $x_i = i / M / 10, i = 1,2,...,10$, $j = 1$.

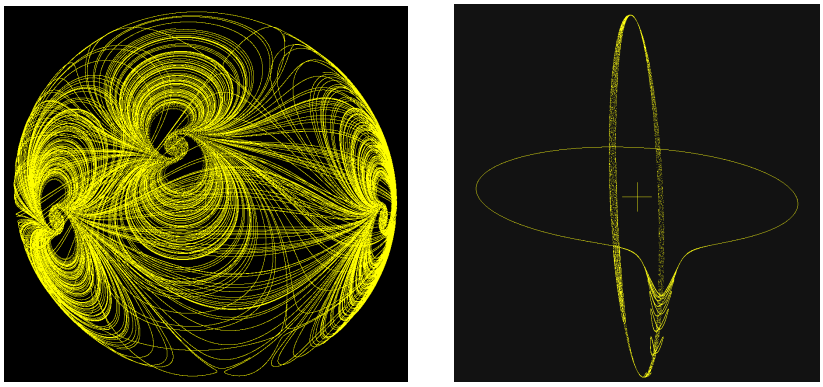

Fig. 12. Left: dipole patterns from random starts, power -2, $M = 3$, EC = (1,-1, 1), $k = 4$, $j = 1$. Right: $\vartheta_t(\theta_t)$ with EC = (1, 1, 1), chaotic core, power -2, $M = 13$.

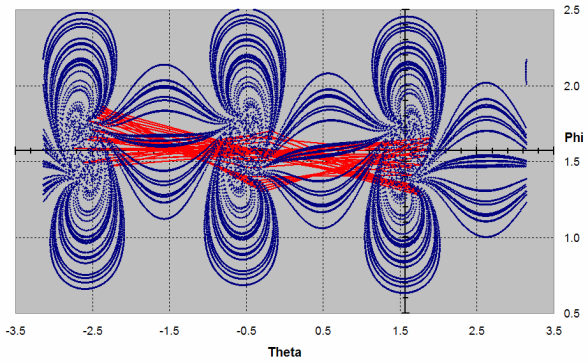

Fig. 13. Dipole pattern mapped to the rectangular phase space, power -2, $M = 3$, EC = (1,-1, 1), $k = 3$, $j = 1$ after 32000 steps. Red are some jump path lines.

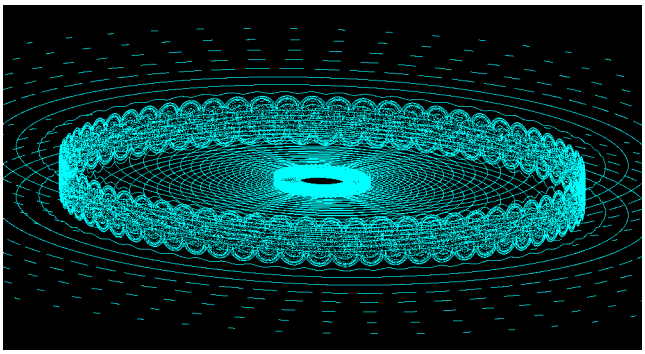

Fig. 14. $M = 128$, $k = 1$, EC = (1, -1, 1), radial variation, $d = (2,0)$

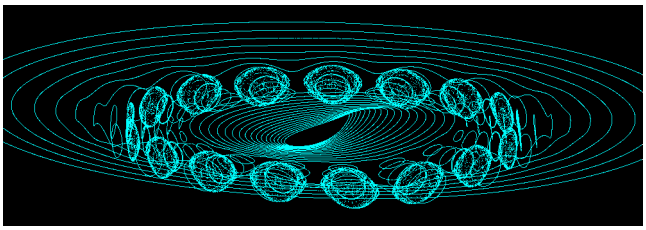

Fig. 15. $M = 20$, $k = 2.3$, EC = (1, 1, 1), radial variation, $d = (2,0)$

4.f Higher-Dimensional Rotated-Rotations

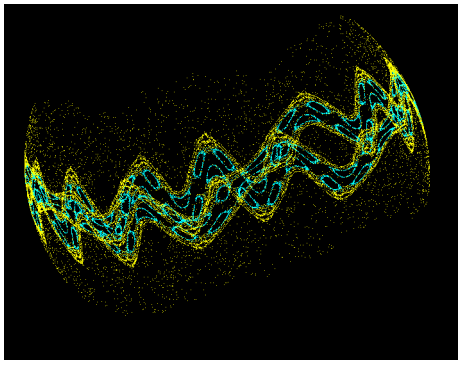

Fig. 16. $n = 3$, $k = 2$, EC = (1, -1, 1), angular variation, $d = (2,2,2)$

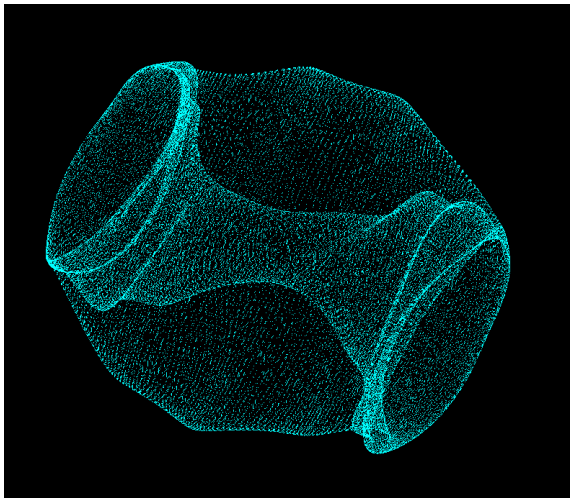

Fig. 17. n = 4, 3-D Projection, k = 1, EC = (1, -1, 1,-1)

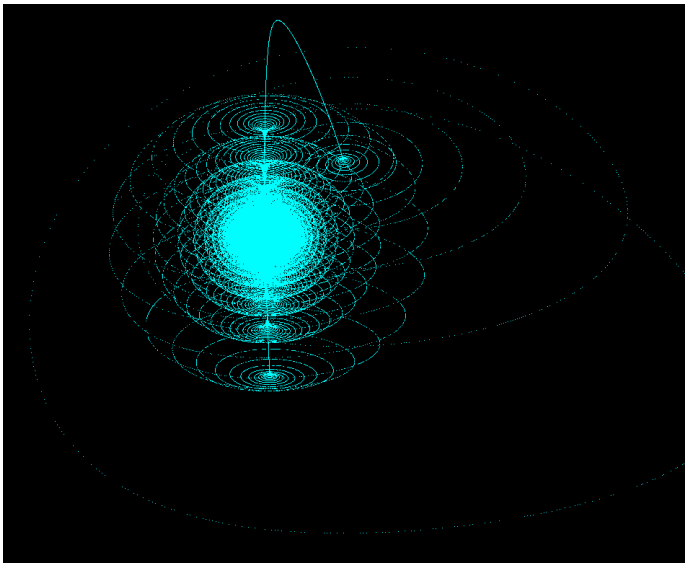

Fig. 18. n = 4 , 3-D Projection, k = 12, EC = (1, -1, 1,-1), d = (3,0,3,0)

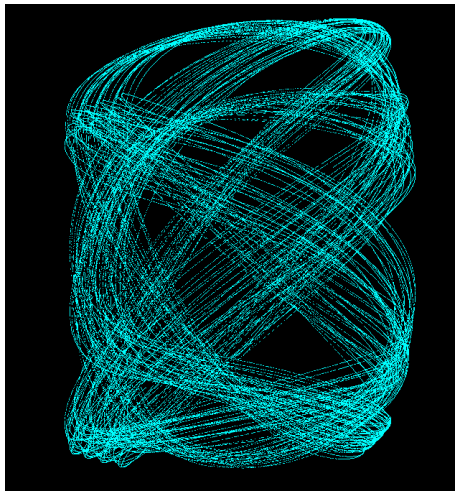

Fig. 19. $n = 5$, 3-D Projection, $k = 1$, EC = (1, -1, 1,-1,1), d = (4,0,4,0,4)

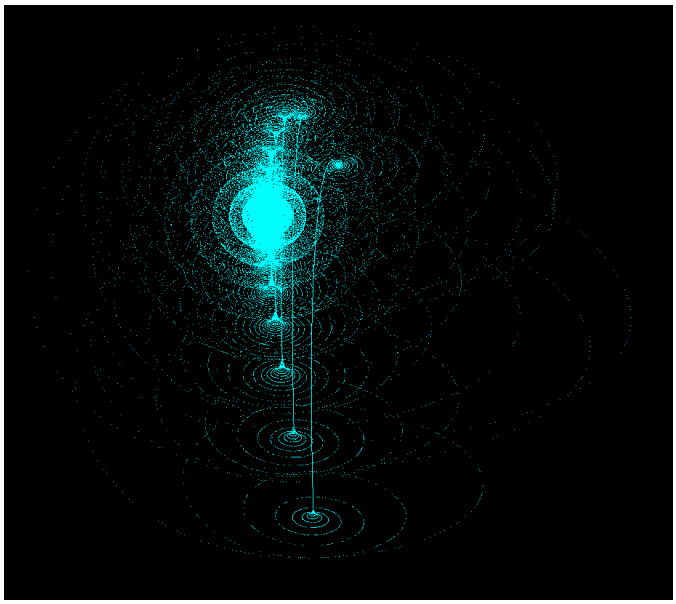

Fig. 20. $n = 6$, 3-D Projection, $k = 6$, EC = (1, -1, 1,-1, 1,-1), d = (5,0,5,0,5,0,5)

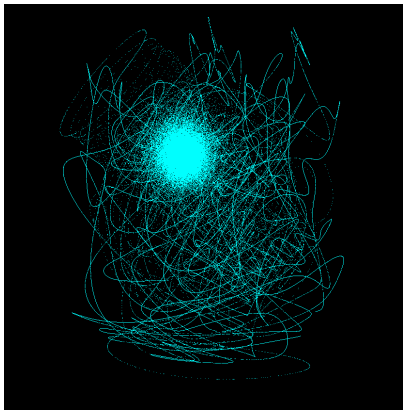

Fig. 21. n = 10, 3-D Projection, k = 12, EC = (1,1,1,1,1,1,1,1,1,1), d = (9,9,9,9,9,9,9,9,9,9)

5. Measure of Chaos/Exponents

Since the map can be extended to an arbitrary number of dimensions n and singularities, we can have a higher-dimensional chaos located in or on hyper-spheres with rotation axes defined by hyper-planes, so it could be called hyper-chaos [5,6] or hyper-sphere chaos. As a measure of chaos we have computed the mean space trajectory separation exponent in n-D between two nearby vectors $\mathbf{p}_{1,t}, \mathbf{p}_{2,t}$ for one complete n-D iteration step during the time τ averaging $0 < i < I$ successive steps with $t = i\tau$

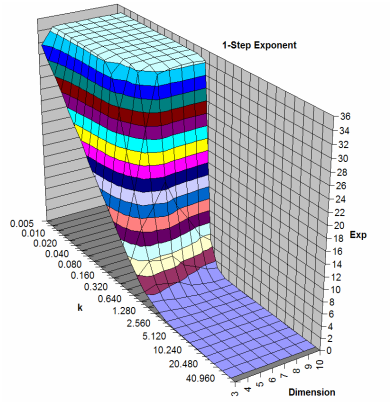

Fig. 22. The 1-step exponent E_τ for n = 3,4,…,10 dimensions and I = 500

$$E_\tau = \frac{1}{I}\sum_{i=0}^{I-1} \log\left[\left|\mathbf{p}_{1,t+(i+1)\tau} - \mathbf{p}_{2,t+(i+1)\tau}\right| / \left|\mathbf{p}_{1,t+i\tau} - \mathbf{p}_{2,t+i\tau}\right|\right], \qquad (14)$$

which is a cheap estimate of the Lyapunov exponent. This exponent is highly stable and increases with the number of dimensions n and with the amplitude/strength factor k of rotation, see fig 24. In our simulation the 1-step exponent E_τ was in our case limited to about 35 due to the double precision limit of the floating point computing unit. It starts to increase strongly near to the control parameter value k = 0.5, see eq.(12). There the pattern becomes "randomized" and chaotic especially at higher hyper sphere rotation dimensions. At higher exponents we find that the map is a good pseudo-random number generator in any dimension $n > 2$. Fig. 22 was obtained without expansion or compression EC = (1,1,1, ...) like all of shown patterns in all figures. With compression-reflection coefficients smaller 1 like EC = (0.99,0.99,0.99, ...) we get negative exponents for $k >> 0.5$ and in-spiralling towards the centre.

6. Cryptography with Hyper-Chaos on the Hyper-Sphere

The rotations $\mathbf{R}_{a,b}$ part of the global sequence $\mathbf{R}_{A,B}$ do not commute, so the time ordering is crucial. The non-commutative permutations of the non-abelian group elements are relevant for encryption purposes. If the permutation is a sequence with a selection of K elements out of $L = N(n\text{-}2) = n(n\text{-}1)(n\text{-}2)/2$ rotations that contains each element once, the number of combinations is given by $C = L!/(L-K)!$. Knowing the rotation angles $\vartheta_{a,b,l}$ and the global sequence $\mathbf{R}_{A,B}$, the rotation can only be reversed by applying the rotations and expansion/reflections part of $\mathbf{R}_{A,B}$ in reversed order. This is an encryption given by a rotation permutation from a series of linked non-commuting mathematical operations, where decryption is done by simply reversing the process applied to signal packages containing some bits of information. The key complexity defining the variations in the rotation sequence would be given by the permutation of combinations. In addition there is the freedom to choose the rotation angles, the initial condition in the signal $\mathbf{p}_0 = \mathbf{p}_t(t=0)$, and the singularity locations $\mathbf{s}_{a,b,l}$ with given precision. Secret key sharing could be done by hiding the initial conditions $\mathbf{p}_0 = \mathbf{p}_t(t=0)$, the singularity locations $\mathbf{s}_{a,b,l}$, and eventually some rotation axes $\mathbf{X}_b$ with Blakley's scheme from the intersection of distributed planes $\mathbf{P}$ [7], where any of the N nonparallel 2-dimensional hyperplanes intersect at a specific point or axis, and each participant is given enough information to define one of the hyper-planes $\mathbf{P}$. Of course, key-shifting during the sequence could also be introduced, which could be done by mobile singularities providing for extreme confusion and diffusion properties. Thus reversibility is practically limited to a small number of encryption/decryption operations due to a limited calculation precision and the high exponential divergence and pseudo-randomness, see fig. 24.

7. Mobile Singularities Exchanging Momentum Quanta

Up to now the simulated singularities had a static location. But a physical situation usually requires mobile singularities.

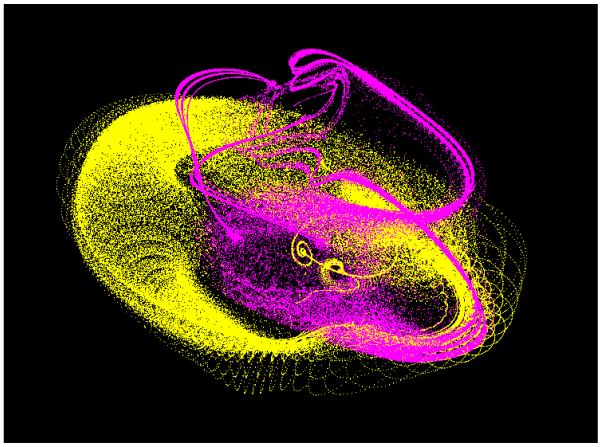

Fig. 23: Two massive mobile singularities generating and absorbing yellow and pink signals carrying momentum and providing for a vector-field.

An important extension would be given by mobile singularities $\mathbf{s}_{a,c,l} \to \mathbf{s}_{a,c,l}(t) = \mathbf{s}_{t,a,c,l}$ or mobile rotation axes carrying momentum like spinning particles with spin – orbit coupling. In the real world the emission or absorption of a rotation-translation or rotation-rotation signal would transfer a linear or angular momentum quantum to and from the singularity if it has a nonzero angular momentum. In addition to the various possibilities to introduce local rotations and accelerations from distance-dependent interactions between singularities is to provide for an extra rotational interaction dynamics between two mobile singularities $\mathbf{s}_{t,a,c,l}$ and $\mathbf{s}_{t,b,c,l}$, there could be a common rotation $\bar{\mathbf{R}}_{t,c}(\bar{\vartheta}_{t,c})$ with common axis $\bar{\mathbf{X}}_c$ (length is the rotation angle) performing the interaction of singularities. Here are two possibilities:

(1) parallel to one of the rotation axes $\bar{\mathbf{X}}_c \parallel \mathbf{X}_a$ or $\bar{\mathbf{X}}_c \parallel \mathbf{X}_b$ or

(2) orthogonal to the interacting singularities rotation axis $\bar{\mathbf{X}}_c \perp \mathbf{X}_a \perp \mathbf{X}_b$, $\bar{\mathbf{X}}_c = \mathbf{X}_a \times \mathbf{X}_b$ having SO(3) symmetry with new interaction singularity located on the intersection of the three axes.

To get something like a mass or providing for inertia and angular momentum a density of visited points after many jumps at time t or spatial sampling function dependent on the initial conditions $\rho_{t=0}$ could be defined by

$$\rho_{t=I\tau}(\mathbf{x}) = \frac{1}{I}\sum_{i=0}^{I-1}\delta(\mathbf{x}-\mathbf{p}_{i\tau}) . \tag{15}$$

With the expanded density by $\tilde{\rho}_t = \mathbf{E}[\rho_t]$, $\mathbf{E}^{-1}[\tilde{\rho}_t] = \rho_t$ we get the difference operator equation $\mathbf{R}_{A,B}[\tilde{\rho}_t] = \mathbf{E}^{-1}[\tilde{\rho}_{t+\tau}]$. Equilibrium is approached for $\tilde{\rho}_t \approx \tilde{\rho}_{t\to\infty}$.

8. Discussion

How do patterns emerge from eq.10? At the present stage we just start to explore the very rich system of pattern formation from map parameter and initial value customization. Without systematic approach this task is hard to do. A basic pattern property at lower dimensions can be assigned to the sign of the reflection exponent, a negative sign leads to an up/down oscillatory behaviour in the jumps shaping the pattern in the altitude, see fig. 13. In the other direction the orbital loops with $\theta_{j,M} = 2\pi j / M$ around axes at coupling exponent $d = 0$ can provide at any radius M/j orbital jump position that are only slightly shifted after every loop, see figs 9-16. At higher dimensions even at high k-values (see figs 19, 21, and 23) the patterns look often more random than the nice structures and symmetries that can be easily obtained at lower dimensions, see figs 1-16. In 4, 5, and 6 dimensions we found interesting structures just by trial, see 17-20. The Skiadas singularity rotation varies with radial distance to the singularity and coupling factor or rotation strength $1/k$ as an important tuning parameter to obtain the pattern structures, see figs. 12-15 and 22. The smaller k, the higher the extra rotation providing for a more nonlinear behaviour and chaotic or even pseudo-random stochastic structure in the pattern, especially near the equatorial location of the singularity, see fig. 12 right. Subject to periodic boundaries and closed loop/orbits our chaotic jump functions show especially at higher k values in the non-chaotic regime ($k >> 1$) a small chaotic core at the centre. At strong rotations the divergence and exponents can grow unbounded, see fig 22, leading to pseudo-random patterns. Due to the singularity on the orbit there is no perfect rotational M-gonal symmetry, the angular parts are slightly different, most different is the orbital part where the singularity is located, see fig. 13, where every dipole has a slightly different shape, especially the chaotic core is different.. Smaller shifts produce traces and linear flows with basic symmetries known from other fields. At special values of j, k, and initial conditions we get almost M-independent regular structures like rings and waves or dipole type flows, see figs 9-15.

It can be found that the path and singularity determines the shift, which is typical for geometric shifts or phases. In physics this extra shift is known as a geometric phase emerging on curved surfaces. In [8] we have presented a strange attractor involving geometric phases from three rotations on the sphere, where a linear rotation – translation coupling (rolling or helical paths) provides for simplifications with very interesting holonomic attractor singularities from iterations. We think that the geometric phase interpretation and correspondent phase shift concepts are also valid here, but near to the singularities or "monopole charges" the geometric phase extra rotation is small compared to the

singularity rotation. Since sum of the rotations given by the rotation vector field provides for a vector potential it is not surprising that the patterns at small coupling strengths and far away from singularities look like iso-potential lines for inverse power interaction laws, in fig.9 for a magnetic dipole chain and in fig.10 for a shear flow or pendulum chain. For smaller couplings $1/k$ we get the some rather linear physical properties:

- monopoles and dipoles (dipole see fig. 1b and chain in fig. 9),
- twistorial spin (vortex structures, see fig. 1 and 20, helical twist fig. 6),
- parity properties and even/odd symmetries (see figs. 3-5),
- j and M could be interpreted as spin and orbital number, respectively,
- inbuilt constant propagation velocity in the translation or rotation in eq. (2),
- Gauss flux exponent d in $n = d + 1$ dimensions,
- wave/particle duality with discrete jumps providing for density patterns,
- scalar and vector fields with standard gauge symmetries,
- angular momentum transfer, interaction and kinetic energy.
- hierarchy of patterns, see figs. 18 and 20,

Opening the loop and translating it into a helical path keeps the basic pattern units if proper periodic boundaries with reflection are introduced. Remarkably, periodic rotation-rotation dipole-dipole interaction patterns emerge on the spherical or helical loop, where the characteristic flux lines are emitted from a chaotic core, see figs. 9, 12-16. Dipole chain patterns play a very important role for living organisms since the molecular dipole interaction leads to protein folding. “Every process of protein formation, from the binding of individual amino acids to secondary structures to tertiary structures and even the formation of quaternary structures is dependent on dipole-dipole interactions [9].”

4-D patterns projected to 3-D show often torus shapes, see fig. 17, typically relevant to Hamiltonian system of spin-spin and spin-orbit coupling. Spin(n) is simply connected and so coincides with the universal cover of SO(n) with isomorphisms and decompositions among the classical Lie groups like Spin(2) = U(1) = SO(2), Spin(3) = SU(2), Spin(4) = SU(2) x SU(2), SU(4) = Spin(6). So Spin(2) and Spin(3) structures can be embedded together in Spin(4). The same can be done in arbitrary high dimensions providing in our case for interplay of low-dimensional ordered states part of a higher-dimensional chaos. This could point to a kind of “itinerancy” [10]. Figs. 18 and 20 show connected (by thin wormholes) lower-dimensional chaotic structures embedded in 4-D and 6-D higher-dimensional systems with very low LE in the projection to three dimensions. This could have relevance to the standard model high energy particle physics with separable but interconnected subgroups in the 10-D gauge field embeddings $\mathrm{SU}(3)\times\mathrm{SU}(2)\times\mathrm{U}(1) \subset SU(5)$ [4].

Introducing mass and momentum, mobile singularities emitting and absorbing the jumping chaotic signal quanta carrying momentum and travelling at constant

speed provide for a very rich chaotic behaviour and dynamics, see the special example in fig. 23.

9. Conclusions

We conclude that using an iterative reflection-rotation-rotation/translation difference equation modelling approach according to Skiadas we can obtain many new interesting patterns with attributes similar to those known from physics. The multiple rotation formula generating hyper-sphere chaos can be extended to an arbitrary number of dimensions, rotations, and singularities. Mobile singularities could even produce more chaos. If the singularity is located at very large distances a small rotation can approximate a translation. At special numbers with smaller coupling $1/k$ and special initial conditions regular structures like rings, spirals, and waves or the many dipole-dipole interaction flows emerge, which could be promising for molecular science and new basic level concepts. Important for a pattern generation on the orbit is a tiny but nonlinear shift in both angular variables due to a cyclic and path dependent singularity extra rotation that is small compared to the orbital angular steps and more linear at smaller coupling (higher k) values. The hyper-sphere chaos from rotation permutations could act as a pseudo-random generator of chaotic patterns relevant for crypto applications with key given by initial conditions and the special rotation permutation sequence in higher dimensions.

References

1. C. H. Skiadas and C. Skiadas, Chaos in Simple Rotation-Translation Models, http://arxiv.org/abs/nlin/0701012, nlin.CD, 2007.
2. C. H. Skiadas and C. Skiadas. *Chaotic Modeling and Simulation: Analysis of Chaotic Models, Attractors and Forms*, Taylor and Francis/CRC, London, 2008.
3. C. H. Skiadas, Von Karman Streets Chaotic Simulation, *Topics on Chaotic Systems*, C. H. Skiadas, I. Dimotikalis and C. Skiadas, (Eds), World Scientific, 309-313, 2009.
4. M. Kaku, *Hyperspace: A Scientific Odyssey Through Parallel Universes, Time Warps, and the Tenth Dimension*, Oxford University Press, 1994.
5. O.E. Rössler, „An equation for hyperchaos“, Phys. Lett. A 71, 155, 1979.
6. G. Qi, D. L. Owuor, A. E. Botha, Robustness and Bit Error Rate Performance of Qi Hyper Chaos Based Encryption, *CHAOS2012 Proceedings*, C. H. Skiadas, I. Dimotikalis, and C. Skiadas, (Eds), 2012.
7. G. R. Blakley, "Safeguarding cryptographic keys". Proceedings of the National Computer Conference 48, 313–317, 1979.
8. B. Binder, Magic Angle Chaotic Precession, *Topics on Chaotic Systems*, C. H. Skiadas, I. Dimotikalis, and C. Skiadas, (Eds), World Scientific, 31-42, 2009.
9. Chem Wiki for Dipole-Dipole Interaction, http://chemwiki.ucdavis.edu, search “Dipole-Dipole_Interactions”, accessed 5.5.2012.
10. K. Kaneko, I. Tsuda, “Chaotic Itinerancy”, Chaos 13(3), 926-936, 2003.